DYNAMIC VERSUS STATIC COMPUTATION OF
THE RESIDUAL CAPACITY OF A MAINSHOCK-DAMAGED BUILDING
TO WITHSTAND AN AFTERSHOCK

Nicolas LUCO[1], Paolo BAZZURRO[2], and C. Allin CORNELL[3]

SUMMARY

The residual capacity against collapse of a mainshock-damaged building can be coupled with the aftershock ground motion hazard (demand) at its site to make an objective decision regarding the occupancy of the building based on its probability of collapse in an aftershock. For a case-study building, a relatively simple nonlinear static-pushover approach to computing residual capacities is found to underestimate the median results of more accurate nonlinear dynamic analyses. By reflecting the dependence observed from the dynamic analyses of residual capacity on residual roof drift, a "calibrated" static approach is proposed that computes more consistent residual capacities.

INTRODUCTION

In the aftermath of a major earthquake, structural engineers must assess whether damaged buildings can continue to be occupied, with due consideration to the threat of aftershocks. An objective and quantifiable criterion that can be used to green/yellow/red-tag a damaged building is the probability (within a specified time period) of its localized or complete collapse in an aftershock. Computing this collapse probability can be accomplished by convolving the aftershock ground motion hazard (demand) at the site, e.g., [1], with the probabilistic residual capacity of the damaged building to withstand aftershock shaking (i.e., its "aftershock fragility"). The residual capacity can be computed via nonlinear structural analyses, e.g., [2,3,4,5], but if a tagging decision needs to be made soon after the mainshock, such analyses should be conducted *a priori* for a range of potential post-mainshock damage states.

As part of Phase I of a project for the Pacific Earthquake Engineering Research Lifelines (PEER-LL) Program and Pacific Gas & Electric, Bazzurro *et al.* [6] have developed guidelines for tagging that involve nonlinear structural analyses performed prior to a mainshock to determine the residual capacity of a given building in several different states of potential damage. To be more practical, the guidelines call for a static-pushover (SPO) analysis and the use of a tool called SPOIDA [7,8] to infer dynamic response rather than carrying out more accurate nonlinear dynamic analyses (NDA's). Phase II of the PEER-LL project has been to verify whether the results of the "static" computations called for in the guidelines are

---

consistent with those of a dynamic approach involving back-to-back NDA's of the building model for numerous mainshock and aftershock pairs of earthquake records. Part of this verification phase is summarized in this paper. For a summary of the guidelines by Bazzurro *et al.* [6], refer to the 13WCEE paper 1708 [9].

OBJECTIVES

The general objectives of this paper are three-fold: (i) to demonstrate for a case-study building the dynamic and the static approaches to computing the residual capacity of a mainshock-damaged building, (ii) to compare the results of the dynamic and the static computations, and (iii) to use the results of the dynamic approach to calibrate the static approach. In all of the approaches, residual capacities are computed for a range of potential post-mainshock damage states obtained via static or dynamic analyses.

CASE-STUDY BUILDING

The building considered in this paper is borrowed from one of the case studies presented in the guidelines by Bazzurro *et al.* [6]. The building is a 3-story steel moment-resisting frame (SMRF) constructed in San Francisco in 1989. It is roughly symmetric, so only one of its 3-bay MRF's is modeled. The beam-column connections are modeled as brittle, with fracture occurring at a plastic hinge rotation of 0.03 radians, at which point the moment strength drops to 30% of the plastic value. A static pushover (SPO) curve for the building model computed using the RAM-Perform V1.04 [10] structural analysis program is shown in Figure 1. The SPO analysis is ceased when the first shear-tab fails, which is assumed to occur at a plastic hinge rotation of 0.07 radians. At this point of local collapse, the SPO curve is assumed to drop to zero base shear.
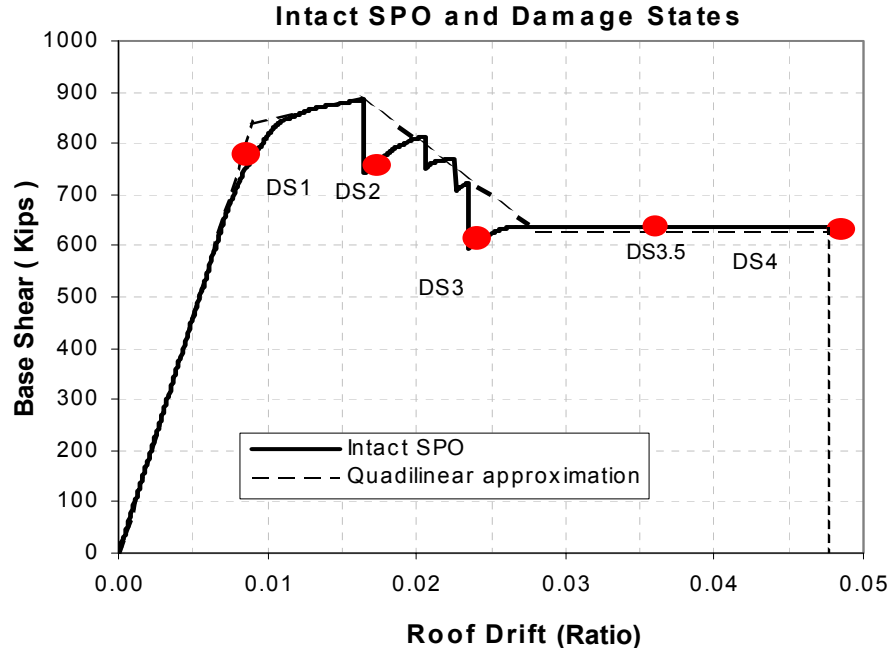

Figure 1. Nonlinear static-pushover (SPO) curve for the intact, or undamaged, three-story SMRF case-study building. The quadrilinear approximation is the SPO curve for the SDOF idealizations of this first-mode dominated building that are analyzed in this paper. The five post-mainshock damage states considered are also identified. This figure was excerpted, with few modifications, from [6].
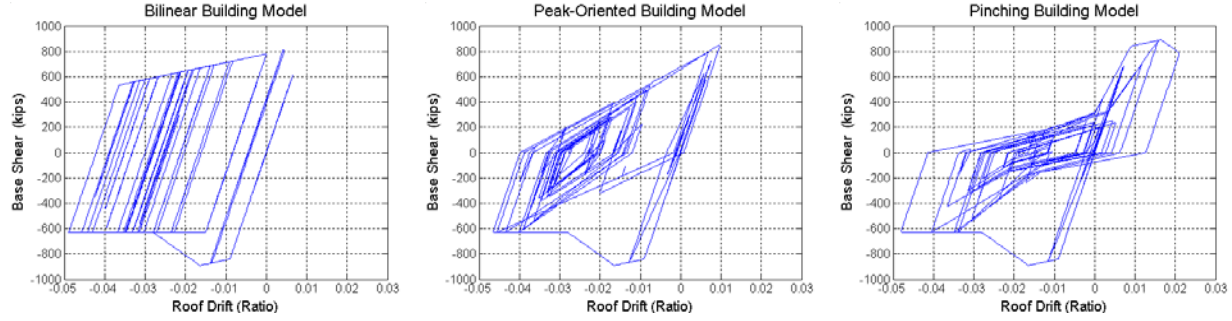
Figure 2. Examples of the hysteretic behavior of the bilinear, peak-oriented, and pinching SDOF building models analyzed in this paper. The backbone for all three models is the same as the quadrilinear approximation of the SPO curve for the first-mode dominated case-study building (shown in Figure 1).

Mainly because the dynamic computation of residual capacity involves a large number of NDA's, three single-degree-of-freedom (SDOF) idealizations of the first-mode-dominated 3-story building model described above are analyzed in this paper. All three SDOF building models have the same fundamental period (T_1=0.73s) and approximately the same force-deformation backbone curve (see Figure 1) as the full multi-degree-of-freedom (MDOF) building model. The three SDOF models differ only in their hysteretic behaviors. As illustrated in Figure 2, the hysteresis rules considered are bilinear, peak-oriented (or "Clough" [11]), and pinching, which are the three options available in the SDOF time-history analysis program used [12].

POST-MAINSHOCK DAMAGE STATES

The five post-mainshock damage states considered for the case-study building are identified on its SPO curve in Figure 1 above. Note that DS1 corresponds to the onset of damage, so in this state the building is still in its intact, or pre-mainshock, condition. At the opposite end of the range of potential damage states, DS4 corresponds to collapse, or in this case local failure of a shear-tab. As defined in the guidelines case-study by Bazzurro *et al.* [6,9], DS2 and DS3 correspond to fracture of the exterior and interior beam-column connections at the first floor, respectively. The intermediate DS3.5 is added in this paper without regard to the corresponding physical damage, but it could be determined from the SPO results. These descriptions of physical damage could be used by an inspector to determine which damage state the case-study building is in after an earthquake.

Also based on the SPO results, each post-mainshock damage state is linked to a peak (during the mainshock) roof drift, as illustrated in Figure 1 above and summarized in Table 1 below. For the SDOF models of the case-study building, these peak roof drifts are synonymous with the associated post-mainshock damage states. In fact, in this paper the results for each damage state are usually plotted versus the corresponding peak roof drift. To estimate results for damage states not considered in this paper, one could interpolate between the corresponding peak roof drifts.

Table 1. Peak roof drift (normalized by roof height) associated with each of the five post-mainshock damage states identified in Figure 1 on the SPO curve for the case-study building.

Peak Roof Drift (Ratio)				
DS1 (Intact)	DS2	DS3	DS3.5	DS4 (Collapsed)
0.009	0.016	0.024	0.036	0.048

DEFINITION OF RESIDUAL CAPACITY

In the guidelines by Bazzurro *et al.* [6,9], the residual capacity of a building in a given post-mainshock damage state is defined as the smallest ground motion spectral acceleration (at T_1 and a damping ratio of 5%) that would induce localized or complete collapse in an aftershock. This residual capacity is a random quantity in the sense that it varies across potential aftershock ground motions (among other things). In this paper, only the medians (calculated as the geometric means) of the residual capacity as computed via the dynamic and static approaches are compared. Although not reported here, the dispersion of the residual capacity, which can be coupled with the median to arrive at the "aftershock fragility" of a mainshock-damaged building, has also been computed.

DYNAMIC COMPUTATION OF RESIDUAL CAPACITY

The dynamic approach to computing the median residual capacity of a building in each post-mainshock damage state involves the following steps:

1. Obtain multiple realizations of the building in each post-mainshock damage state by performing NDA of the intact building model subjected to multiple mainshock ground motions, each one scaled (in amplitude only) to induce the roof drift associated with each damage state.
2. Compute residual capacities for each of these realizations of the building by subjecting them, via NDA, to aftershock ground motions scaled to induce the roof drift associated with collapse.
3. Calculate the median residual capacity for each damage state over all the pairs of mainshock-damaged building realization (Step 1) and potential aftershock ground motion (Step 2).

The details of these steps and their results for the three SDOF models of the case-study building are discussed in the subsections below. To simplify the comparison of results from this dynamic approach with those from the static approach presented in the next section, the same 30 earthquake recordings used by Vamvatsikos [7,8] in developing the SPO2IDA tool are also used here. Furthermore, this single set of earthquake recordings is used to represent both potential mainshock and aftershock ground motions. If, instead, different sets of earthquake recordings are used to represent mainshocks and aftershocks, the median residual capacity for each damage state may change, but its value relative to that for DS1 (e.g., see Figure 9 below) is expected to remain the same.

Step 1: NDA of intact building subjected to mainshocks
In addition to multiple realizations of the building in each post-mainshock damage state, three by-products of the NDA's of the intact building model subjected to multiple mainshock ground motions are (i) incremental dynamic analysis (IDA) curves, (ii) residual roof drifts in each damage state, and (iii) capacities against collapse of the intact building. These results are noteworthy because (i) the IDA curves depict the mainshock spectral accelerations that lead to each damage state, which can be used before an earthquake has occurred to compute the annual probability of experiencing each damage state [6,9], (ii) the residual roof drifts have an effect on the residual capacities, as demonstrated later in this paper, and (iii) the intact capacities serve as a basis of comparison for the residual capacities. The three by-products are also results of the static approach demonstrated in the next section. In the section after the next, those static results are compared with the dynamic results summarized in the subsections below.

IDA Curves
Scaling an earthquake record to obtain a realization of the building in each post-mainshock damage state is an iterative process not unlike computing a constant ductility response spectrum. The first by-product of this iterative scaling is an IDA curve that relates the spectral acceleration of the ground motion (proportional to the scale factor) to the peak roof drift of the building. Figure 3(a) shows, for the
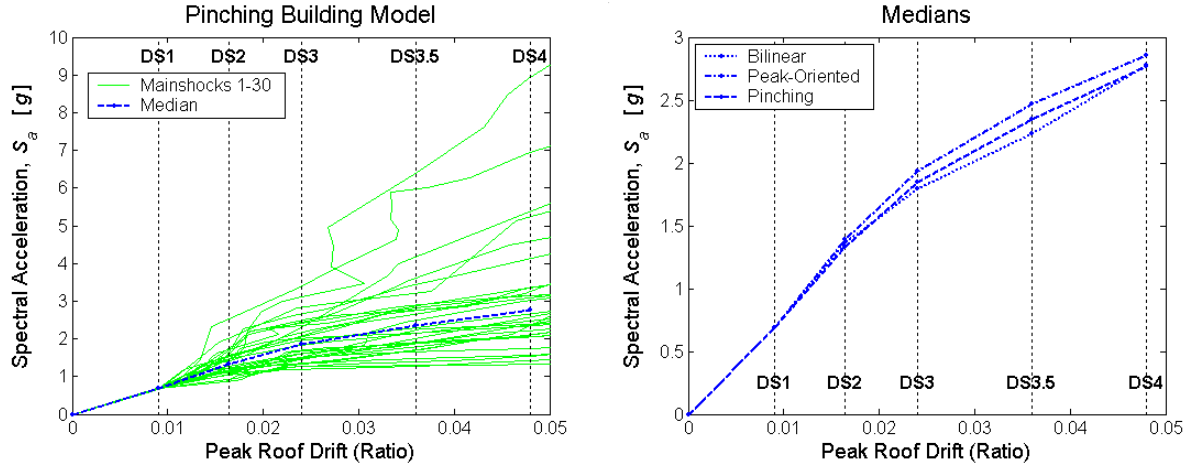
Figure 3. **Incremental Dynamic Analysis (IDA) curves computed while obtaining multiple realizations of each post-mainshock damage state. Panel (a) shows, for the pinching building model, the individual IDA curves for the 30 mainshock ground motions considered. Panel (b) shows the median IDA curves across the 30 mainshocks for all three of the case-study building models.**

pinching model of the case-study building, the 30 IDA curves obtained for the 30 "mainshock" earthquake records. Also shown in Figure 3(a) is a median IDA curve established by connecting the median spectral accelerations that induce the peak roof drifts associated with the five damage states. The median IDA curves for the bilinear, peak-oriented, and pinching building models are shown in Figure 3(b). Note their similarity despite the differences in hysteretic behavior.

Residual Roof Drifts
Each earthquake record that is scaled to induce the peak roof drift associated with a post-mainshock damage state will also induce a residual roof drift. For the 30 mainshock earthquake records and the pinching building model, the residual roof drifts (absolute values) in each damage state are plotted in Figure 4(a); also plotted is a curve connecting the median residual roof drift values for the five damage states. The median residual roof drifts for all three building models are plotted in Figure 4(b).
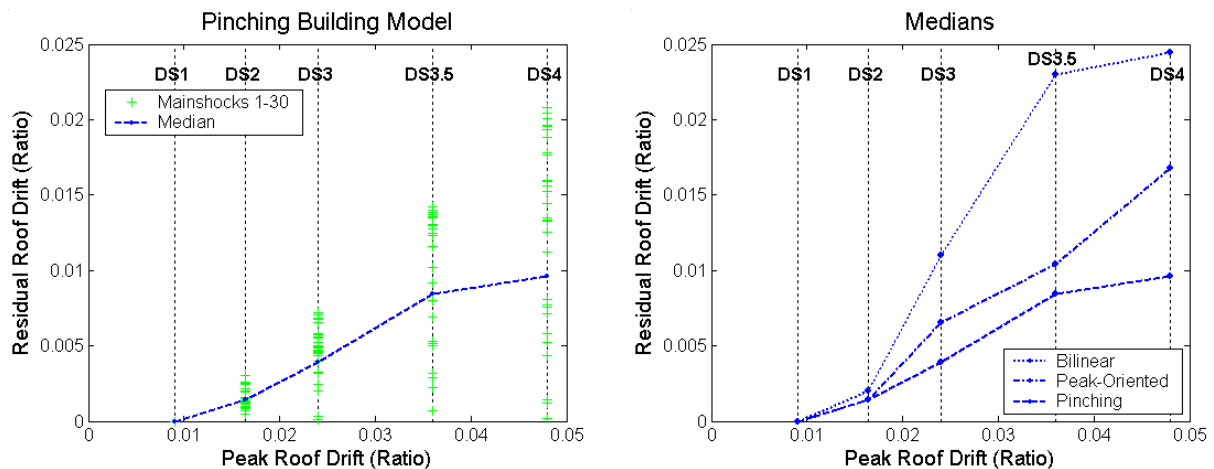

Figure 4. **Residual roof drifts for each post-mainshock damage state (or associated value of peak roof drift). Panel (a) shows, for the pinching building model, the residual roof drifts caused by the 30 mainshock ground motions considered. Panel (b) shows the median residual roof drift across the 30 mainshocks for all three of the case-study building models.**

Recall that in DS1 the building is still elastic, so there is no residual roof drift. As the damage (or peak roof drift) increases, so does the median residual roof drift, particularly for the bilinear building model. The stiffness reductions in the peak-oriented and pinching hysteresis loops have a "self-centering" effect that leads to relatively small residual drifts, as observed by other researchers as well, e.g., [13,14,15].

Intact Capacities

From each of the median IDA curves in Figure 3(b) above, the spectral acceleration that induces the peak roof drift associated with collapse (i.e., DS4) is the median capacity of the intact building. For the bilinear, peak-oriented, and pinching models of the case-study building, these median intact capacities are 2.78*g*, 2.86*g*, and 2.77*g*, respectively. Like the median IDA curves themselves, the median intact capacities for the three building models are very similar (within 4% of each other). Note that these intact capacities are also the residual capacities in DS1, which provides a convenient basis of comparison for the median residual capacities computed in the next step for the other damage states.

Step 2: NDA of mainshock-damaged building subjected to aftershocks

For each realization of a mainshock-damaged building created in Step 1, residual capacities are computed by performing NDA with aftershock earthquake records, each one scaled to induce the peak roof drift associated with collapse. As for the mainshocks in Step 1, scaling the aftershocks is an iterative process. Unlike the mainshocks, however, scaling the aftershocks by positive and negative factors typically results in two different spectral accelerations (both absolute values) that trigger collapse. The smaller value is kept, since the residual capacity is defined (above) as the smallest aftershock spectral acceleration that induces collapse. Over all of the realizations and mainshocks considered in this paper, the larger of the two spectral accelerations is on average 1.23 times and at most 3.19 times the smaller value.

In effect, back-to-back mainshock-aftershock NDA's are performed in Steps 1-2, as illustrated in Figure 5 for the pinching building model. In this example, the mainshock NDA produces a realization of the building in DS3 (i.e., peak roof drift ratio of 0.024), whereas the aftershock NDA results in collapse (at a peak roof drift of 0.048). The spectral acceleration of the aftershock ground motion is the residual capacity for this particular realization of the pinching building model in DS3. The residual capacities for all 30x30 of the mainshock-aftershock pairs considered are listed in Table 2.

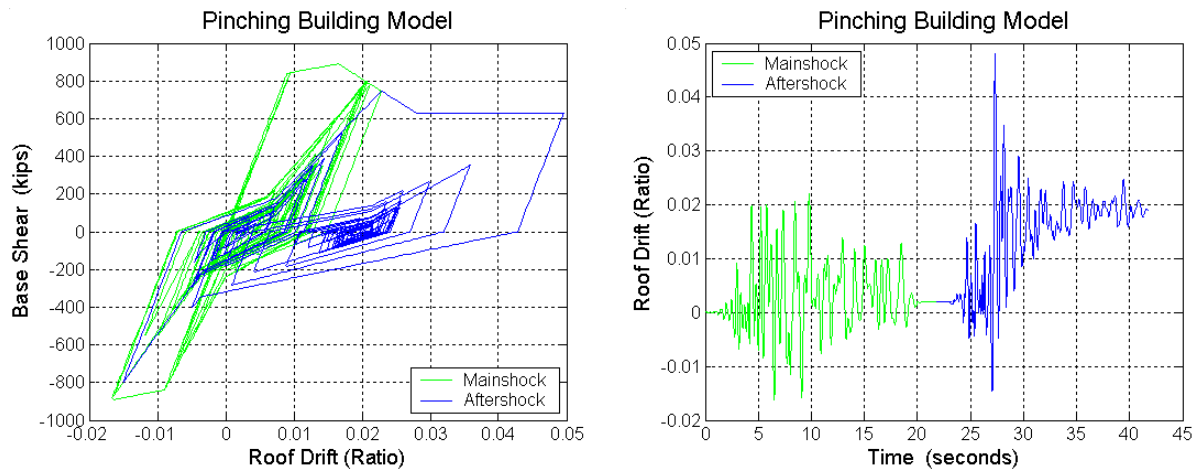**Figure 5. Example hysteresis loops and roof drift time histories from the back-to-back mainshock-aftershock dynamic analyses performed to compute the residual capacity of a mainshock-damaged building. The mainshock ground motion is scaled to induce the peak roof drift associated with DS3, and the aftershock ground motion is scaled to induce the peak roof drift associated with collapse (DS4).**

Table 2. Residual capacities (i.e., minimum spectral accelerations to cause collapse) of the pinching building model in damage state DS3 for the 30x30 potential mainshock-aftershock pairs considered.

Mainshock	Residual S_a Capacity (g) for Aftershock																													
	1	2	3	4	5	6	7	8	9	10	11	12	13	14	15	16	17	18	19	20	21	22	23	24	25	26	27	28	29	30
1	1.68	2.83	3.19	2.10	3.30	2.48	2.95	2.24	2.19	2.09	3.74	2.13	5.41	4.72	1.90	1.04	2.48	1.41	1.34	3.88	2.03	2.37	2.72	7.75	2.18	4.19	2.70	4.03	1.39	2.11
2	1.67	2.73	3.16	1.97	3.25	2.46	2.87	2.24	2.16	2.03	3.37	2.06	5.30	4.12	1.86	1.05	2.48	1.33	1.34	3.71	1.95	2.27	2.68	7.20	2.09	3.99	2.62	4.13	1.43	2.11
3	1.67	2.67	3.14	1.96	3.32	2.46	2.83	2.12	2.19	2.02	3.37	2.06	5.29	4.20	1.84	1.06	2.34	1.32	1.34	3.71	1.96	2.25	2.70	6.80	2.07	4.04	2.65	4.17	1.32	2.11
4	1.72	3.38	3.38	2.10	3.30	2.49	3.97	2.31	2.06	2.47	5.10	2.13	6.34	5.13	2.07	0.95	2.82	1.41	1.42	5.10	2.00	2.37	2.88	8.91	2.55	5.00	2.87	4.05	1.57	2.78
5	1.66	2.63	3.09	1.68	3.25	2.43	2.78	2.00	2.18	1.98	3.37	2.06	5.22	4.17	1.79	1.06	2.25	1.30	1.34	3.64	1.95	2.22	2.66	6.54	2.04	3.95	2.69	3.89	1.27	2.11
6	1.66	2.62	3.09	1.68	3.24	2.43	2.78	2.00	2.18	1.97	3.37	2.06	5.22	4.14	1.79	1.06	2.24	1.30	1.34	3.62	1.95	2.22	2.66	6.94	2.04	3.96	2.69	3.89	1.27	2.11
7	1.68	2.69	3.16	2.00	3.26	2.47	2.86	2.16	2.18	2.04	3.37	2.06	5.32	4.18	1.87	1.06	2.48	1.34	1.34	3.74	1.97	2.28	2.71	7.10	2.09	3.99	2.67	4.16	1.34	2.25
8	1.68	2.74	3.17	2.00	3.26	2.47	2.89	2.24	2.17	2.08	3.59	2.06	5.32	4.15	1.87	1.05	2.48	1.35	1.34	3.82	2.00	2.28	2.69	7.40	2.11	4.00	2.64	4.15	1.36	2.11
9	1.68	2.78	3.19	2.10	3.28	2.48	3.08	2.38	2.17	2.25	3.85	2.13	5.53	5.13	1.90	1.04	2.65	1.41	1.34	4.14	2.05	2.37	2.64	8.28	2.33	4.20	2.74	4.03	1.43	2.27
10	1.70	2.59	3.09	1.94	2.99	2.45	2.78	2.03	2.26	1.97	3.15	2.06	5.25	4.38	1.80	1.09	2.19	1.28	1.34	3.60	2.00	2.27	2.78	6.89	2.06	4.00	2.80	4.10	1.27	2.11
11	1.67	2.75	3.20	2.00	3.25	2.48	3.20	2.45	2.13	2.23	3.95	2.12	5.58	5.13	1.89	1.02	2.69	1.41	1.34	4.14	2.04	2.37	2.65	8.37	2.38	4.71	2.75	3.99	1.43	2.38
12	1.67	2.68	3.15	1.99	3.35	2.46	2.84	2.14	2.19	2.04	3.37	2.06	5.30	4.19	1.86	1.06	2.36	1.33	1.34	3.74	1.97	2.25	2.71	6.92	2.08	3.96	2.66	4.18	1.33	2.11
13	1.67	2.64	3.09	1.73	3.27	2.44	2.80	2.01	2.19	2.00	3.37	2.06	5.25	4.14	1.81	1.06	2.28	1.31	1.34	3.68	1.96	2.23	2.68	6.59	2.05	3.99	2.71	4.11	1.27	2.11
14	1.68	2.74	3.17	2.00	3.26	2.47	2.88	2.24	2.17	2.07	3.56	2.06	5.32	4.17	1.87	1.06	2.48	1.34	1.34	3.79	1.96	2.27	2.70	7.29	2.10	3.99	2.64	4.16	1.35	2.11
15	1.66	2.69	3.09	1.71	3.32	2.43	2.84	2.13	2.15	2.03	3.37	2.06	5.26	4.08	1.84	1.03	2.48	1.32	1.34	3.72	1.93	2.24	2.65	7.00	2.06	4.00	2.63	3.92	1.32	2.11
16	1.67	2.73	3.18	1.98	3.25	2.46	2.98	2.24	2.15	2.14	3.80	2.11	5.38	4.43	1.87	1.03	2.64	1.36	1.34	3.93	2.02	2.29	2.54	7.83	2.17	4.07	2.67	4.11	1.39	2.11
17	1.67	2.65	3.09	1.71	3.28	2.45	2.81	2.02	2.19	2.01	3.37	2.06	5.26	4.15	1.82	1.06	2.27	1.31	1.34	3.69	1.97	2.24	2.69	6.61	2.05	4.00	2.72	4.13	1.27	2.11
18	1.68	2.69	3.15	1.98	3.26	2.46	2.86	2.15	2.18	2.00	3.37	2.06	5.31	4.20	1.86	1.06	2.38	1.33	1.34	3.66	1.96	2.28	2.69	7.05	2.08	4.01	2.66	4.14	1.33	2.11
19	1.68	2.73	3.18	1.99	3.25	2.47	2.93	2.24	2.16	2.12	3.69	2.11	5.33	4.03	1.87	1.04	2.48	1.35	1.34	3.88	2.01	2.28	2.64	7.62	2.12	4.02	2.66	4.13	1.37	2.11
20	1.69	2.70	3.17	2.10	3.27	2.48	2.87	2.24	2.19	2.05	3.37	2.06	5.33	4.21	1.88	1.05	2.48	1.35	1.34	3.76	1.98	2.29	2.72	7.16	2.10	4.01	2.65	4.18	1.35	2.27
21	1.66	2.60	3.09	1.70	3.22	2.42	2.77	2.05	2.17	1.93	3.19	2.06	5.20	4.14	1.78	1.06	2.20	1.29	1.34	3.52	1.95	2.22	2.65	6.91	2.03	3.97	2.68	3.63	1.27	2.11
22	1.67	2.75	3.18	2.10	3.27	2.48	2.94	2.24	2.17	2.12	3.73	2.12	5.37	4.75	1.88	1.05	2.48	1.36	1.34	3.90	2.02	2.30	2.67	7.71	2.15	4.08	2.68	4.14	1.38	2.11
23	1.72	3.44	3.31	2.10	3.28	2.50	3.86	2.37	2.06	2.47	4.80	2.14	6.12	5.13	1.98	0.96	2.81	1.41	1.41	4.91	2.03	2.37	2.80	8.91	2.54	4.89	2.89	4.06	1.51	2.76
24	1.66	2.73	3.19	1.98	3.25	2.45	3.08	2.36	2.14	2.19	3.84	2.12	5.49	5.13	1.93	1.02	2.64	1.41	1.34	4.14	2.03	2.37	2.63	8.17	2.30	4.17	2.71	3.98	1.42	2.30
25	1.75	3.57	3.33	2.10	3.34	2.54	3.84	2.42	2.12	2.47	5.10	2.16	6.17	5.13	2.07	1.00	2.84	1.41	1.42	5.10	2.11	2.43	2.76	8.91	2.67	5.01	2.93	4.13	1.53	2.91
26	1.68	2.66	3.09	1.98	3.30	2.46	2.82	2.04	2.23	2.01	3.37	2.06	5.29	4.22	1.84	1.06	2.28	1.33	1.34	3.67	1.98	2.26	2.72	6.82	2.07	3.97	2.66	4.19	1.31	2.11
27	1.70	3.13	3.23	1.99	3.23	2.49	3.77	2.36	2.06	2.47	4.51	2.12	5.90	5.13	1.94	0.97	2.76	1.41	1.39	4.59	2.01	2.37	2.70	8.91	2.48	4.72	2.83	4.00	1.48	2.70
28	1.67	2.77	3.17	1.88	3.24	2.46	2.89	2.24	2.15	2.06	3.61	2.06	5.30	4.09	1.86	1.04	2.48	1.34	1.34	3.78	1.99	2.27	2.65	7.42	2.09	3.99	2.63	4.12	1.35	2.11
29	1.65	2.64	3.21	1.72	3.21	2.49	3.20	2.40	2.06	2.27	4.08	2.06	5.62	5.13	1.88	0.98	2.72	1.41	1.34	4.14	2.01	2.37	2.65	8.91	2.36	4.69	2.72	3.96	1.44	2.56
30	1.69	2.77	3.18	2.10	3.28	2.48	2.90	2.24	2.20	2.08	3.59	2.13	5.35	4.70	1.89	1.05	2.48	1.36	1.34	3.83	1.98	2.30	2.73	7.43	2.13	4.06	2.68	4.18	1.36	2.11

Note from Table 2 that the residual capacities vary much less across the realizations of mainshock damage (rows of the matrix) than they do across potential aftershocks (columns of the matrix), suggesting that the nature of the mainshock that induces the given damage state (in this case DS3) has relatively little effect on the residual capacity. As discussed later in this paper, what little variation there is across the mainshocks is related to the residual roof drifts. In the next step, the median residual capacity over all 30x30 mainshock-aftershock pairs is computed for each of the three building models and each damage state.

Step 3: Calculate median of residual capacities for each post-mainshock damage state
The median residual capacity over all 30x30 pairs of mainshock-damage realizations and potential aftershocks is reported in Table 3 for the three case-study building models in each damage state. Note that the values for DS1 are equal to those computed for the intact building in Step 1. In DS4, there is no (zero) residual capacity because collapse has already occurred. As expected, the median residual capacity decreases with increasing severity of the damage state, particularly for the bilinear building model. Overall, though, the reductions in capacity may seem to some to be surprisingly small considering the degradation in strength and stiffness. The differences among the three hysteretic models are discussed in the section after the next, which compares the results of the dynamic approach presented in this section with those of the static approach presented next.

Table 3. Median residual capacities (over the 30x30 potential mainshock-aftershock pairs) for the three case-study building models in each damage state. In DS1, the residual capacities are equal to those of the intact building. Once in DS4, the building has no residual capacity against collapse.

Building Model	Median Residual S_a Capacity (g)				
	DS1 (Intact)	DS2	DS3	DS3.5	DS4 (Collapsed)
Bilinear	2.78	2.64	2.09	1.64	0
Peak-Oriented	2.86	2.75	2.52	2.35	0
Pinching	2.77	2.70	2.53	2.35	0

STATIC COMPUTATION OF RESIDUAL CAPACITY

The static approach to computing the median residual capacity for each post-mainshock damage state of a building, as proposed in the guidelines by Bazzurro *et al.* [6,9], involves the following steps:

1a. Obtain a realization of the building in each post-mainshock damage state by performing a SPO analysis of the intact building model up to the peak roof drift associated with the damage state, followed by unloading to zero base shear.
1b. Obtain a SPO curve for the building in each damage state by re-loading the realization obtained in Step 1a up to collapse.
2. Compute the median residual capacity by inputting the SPO curve for each damage state from Step 1b into the SPO2IDA tool for inferring dynamic response.

The details of these steps and their results for the SDOF models of the case-study building are discussed in the subsections below. Note that the results for the bilinear, peak-oriented, and pinching models are identical, because the backbone and un/re-loading rule to/from zero base shear, and hence the SPO curve for each damage state, is the same for all three building models.

Step 1a: SPO of intact building (simulates mainshock response)
The SPO analyses (including unloading) of the intact building model called for in Step 1a, which each produce a realization of the building in one of the post-mainshock damage states, are illustrated in Figure 6 for the SDOF building models. Note that the unloading stiffness is parallel to the elastic stiffness, which is true for all three of the hysteretic models (e.g., see Figure 2). The residual roof drifts for the five post-mainshock damage states that are implied by these SPO analyses are circled in the figure (at zero base shear); their values will be compared with the results of NDA in the next section.

Step 1b: SPO of mainshock-damaged building (simulates aftershock response)
Since the re-loading stiffness for each of the damaged-building realizations obtained in Step 1a is parallel to the elastic stiffness (for all three hysteretic models), Figure 6 also shows the SPO curves for the five post-mainshock damage states. Note that the triangular SPO curve for DS4 is not used in Step 2 to compute a median residual capacity, because collapse has already occurred in DS4.
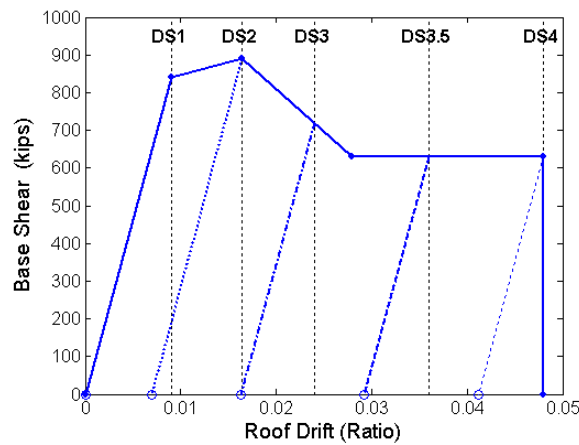

Figure 6. **Static pushover (SPO) curve in each post-mainshock damage state for all three of the SDOF building models considered. Circled at zero base shear are the implied residual roof drifts. The SPO curves are input into the SPO2IDA tool [7,8] to compute the median residual capacities.**
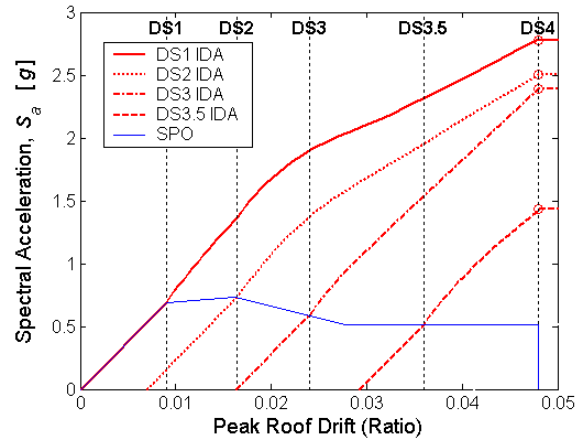
Figure 7. Median IDA curves computed using SPO2IDA [7,8] for each post-mainshock damage state. The curves are the same for all three models of the case-study building. The median residual capacity for each damage state is circled, as given by the spectral acceleration at which each IDA reaches a peak roof drift of 0.048 (corresponding to collapse, or DS4).

Step 2: SPO2IDA for mainshock-damaged building (simulates aftershock response)

SPO2IDA [7,8] is a spreadsheet tool that, as its name suggests, converts a static pushover curve into incremental dynamic analysis curves (median and 16th- and 84th-percentiles). The tool is based on NDA's of numerous SDOF oscillators with various quadrilinear backbone curves and pinching hysteretic behavior, all subjected to the 30 ground motion recordings that are also used in this paper.

Using SPO2IDA, the SPO curve obtained in Step 1 for each post-mainshock damage state (DS1-DS3.5) is translated into a median IDA curve, as shown in Figure 7. The spectral acceleration at the plateau of this median IDA curve, which is also the spectral acceleration that induces the peak roof drift associated with collapse, is the median residual capacity for the damage state. These median residual capacities are circled in Figure 7 and enumerated in Table 4. Note that there is no (zero) residual capacity in DS4, which corresponds to collapse. These results apply to all three of the models of the case-study building, and will be compared with the results of the dynamic approach in the next section.

It should be kept in mind that, although it is used here and in the guidelines by Bazzurro *et al.* [6,9] for such, SPO2IDA was not designed to provide IDA curves for mainshock-damaged buildings with residual roof drifts. Hence, the median residual capacities computed here via the static approach cannot necessarily be expected to agree with the results of the more accurate dynamic approach. In concept, an "aftershock" version of SPO2IDA could be developed using back-to-back mainshock-aftershock NDA's like those performed in the dynamic approach.

Table 4. Median residual capacities for each post-mainshock damage state computed via the static approach. The values are the same for all three models of the case-study building. In damage state DS4, local collapse has already occurred, implying zero residual capacity.

Median Residual S_a Capacity (g)				
DS1 (Intact)	DS2	DS3	DS3.5	DS4 (Collapsed)
2.77	2.50	2.39	1.43	0

COMPARISON OF DYNAMIC VERSUS STATIC RESULTS

Despite their differences, the dynamic and static approaches to computing the median residual capacity of a mainshock-damaged building both generate, as by-products, a median IDA curve and a median capacity for the intact building (i.e., for DS1), and an estimate of the residual roof drift in each post-mainshock damage state. These results from the two approaches, in addition to the median residual capacities for each damage state, are compared in this section.

Median IDA curves and median capacities for the intact building

For brevity, the median IDA curves for the intact building computed via the static (i.e., SPO2IDA) and dynamic (NDA) approaches are not re-plotted here, but a visual review of the intact IDA curve in Figure 7 and those in Figure 3(b) reveals that the two approaches provide nearly the same results. From these IDA curves it is also apparent that the median capacity of the intact building (or the building in DS1) computed via the static approach is close to those computed via nonlinear dynamic analyses. In fact, the median "intact" capacity from the static approach ($2.77g$ – see Table 4) is within 4% of those computed via the dynamic approach ($2.78g$, $2.86g$, and $2.77g$ for the bilinear, peak-oriented, and pinching models, respectively – see Table 3). The results are especially close in part because the same 30 earthquake recordings used by Vamvatsikos [7,8] to develop the SPO2IDA tool are also used here.

Residual roof drifts for each post-mainshock damage state

For each of the post-mainshock damage states (or corresponding peak roof drifts) considered, the residual roof drift implied by the static approach is compared in Figure 8 with the median values computed NDA of the bilinear, peak-oriented, and pinching building models. Note that what is plotted in the figure is the residual roof drift normalized by the peak roof drift associated with each damage state, and hence the ordinate is at most equal to one. Except in DS1, when there is no residual roof drift because the building is elastic, the residual roof drift implied by the SPO curve for each damage state clearly over-estimates the median results of NDA. This is to be expected, since the SPO curves do not allow for the possibility that the building may oscillate in the opposite direction after reaching its peak roof drift. As noted above in the dynamic computation section, the median residual roof drifts from NDA of the bilinear building model are larger than those for the peak-oriented and pinching models, and hence are closer to those implied in the static approach.
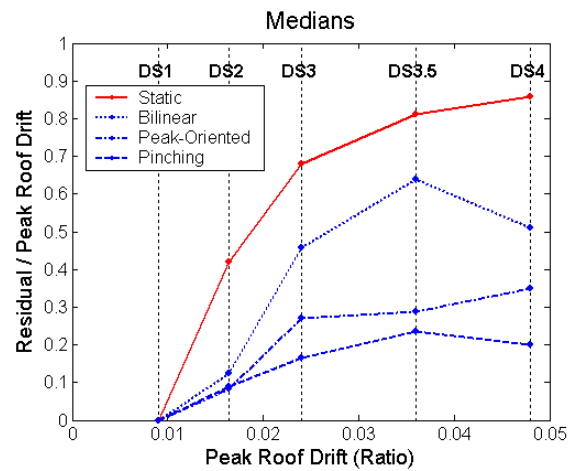

Figure 8. Comparison of (i) the median residual roof drifts (normalized by the peak roof drift) computed via nonlinear dynamic analyses of the three case-study building models with (ii) the residual roof drift implied by the static pushover curve for each post-mainshock damage state.
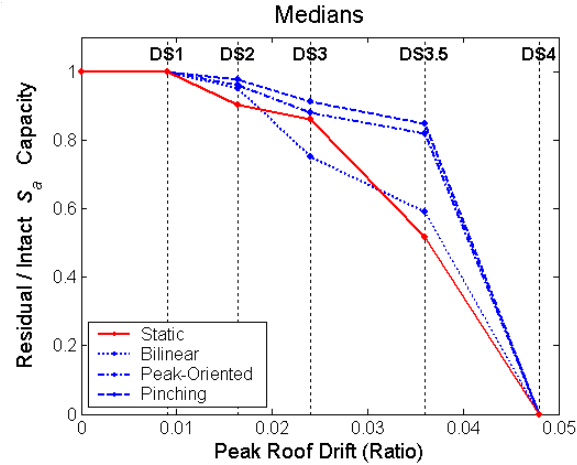
Figure 9. Comparison of the median residual capacities (normalized by the corresponding median *intact* capacities) computed via the static versus dynamic approaches. Recall from Tables 3 and 4 that the median intact capacities (i.e., median residual capacities in post-mainshock damage state DS1) are approximately the same for the three case-study building models whether computed via the static or dynamic approaches.

Median residual capacities for each post-mainshock damage state

The principal results of the dynamic and static computations, namely the median residual capacity for each post-mainshock damage state, are compared in Figure 9. What is actually plotted in the figure is the median residual capacity normalized by the median *intact* capacity (i.e., the median residual capacity for DS1). This residual/intact ratio, which measures the drop in median capacity resulting from mainshock damage, is used in the guidelines by Bazzurro *et al.* [6,9] as a basis for tagging decisions. Note that Figure 9 would look nearly the same if the median residual capacities were plotted instead of the residual/intact ratios, because the median intact capacities computed via the static and dynamic approaches (for all three building models), recall, are approximately the same.

From Figure 9 it is apparent that the static approach generally underestimates the median residual (normalized by intact) capacities computed via the dynamic approach, at least for the peak-oriented and pinching building models. For the bilinear building model, the static results underestimate by a lesser amount, or even overestimate (in DS3), those computed via the dynamic approach. The error in the static computation of median residual/intact capacity, expressed as a percentage of the dynamic result, is provided in Table 5. Note the relatively large error for the peak-oriented and pinching building models in DS3.5. All of the (non-zero) errors are reduced by the calibrated static approach proposed in the next section.

Table 5. Error in the median residual (normalized by intact) capacities computed via the static approach, expressed as a percentage of the more accurate dynamic results also shown in Figure 9. The errors for DS1 are zero because, by definition, the residual/intact ratio is always one. In DS4, local collapse has already occurred, so there are no residual capacities to compute.

Building	Error in Median Residual/Intact Capacity from Static Computation				
Model	DS1 (Intact)	DS2	DS3	DS3.5	DS4 (Collapsed)
Bilinear	0	-5.1%	14.9%	-12.5%	--
Peak-Oriented	0	-6.1%	-2.1%	-37.0%	--
Pinching	0	-8.0%	-5.3%	-39.1%	--

CALIBRATED STATIC COMPUTATION OF RESIDUAL CAPACITY

As shown in the preceding section, overall the results of the static approach are most similar to the dynamic results for the bilinear building model, both in terms of the median residual capacities and the residual roof drifts. This observation, coupled with intuition, suggests that the median residual capacities computed via the static and dynamic approaches might be more similar, particularly for the peak-oriented and pinching building models, if the residual roof drifts were more consistent as well. The median residual roof drifts from the dynamic analyses can be reflected in the static approach by appropriately "shifting" the SPO curve for each damage state obtained in Step 1. As demonstrated below, this shifting is the second step of the "calibrated" static approach.

Step 2: Shift SPO curve for each post-mainshock damage state to "expected" residual roof drift
As an example, in Figure 10(a) the SPO curve for DS2 is shifted back horizontally until its origin is at the median residual roof drift (also in DS2) from NDA of the pinching building model. Note that the roof drift associated with collapse (i.e., 0.048), which is considered an intrinsic property of the building, is not shifted. The resulting median residual capacity computed via SPO2IDA of the shifted SPO curve is larger and, in this example, closer to the value computed via the dynamic approach. For other potential residual roof drifts between zero and the peak roof drift associated with collapse (i.e., 0.048), the resulting median residual (normalized by intact) capacities are plotted in Figure 10(b) for DS2 through DS3.5. Note that each of these plots is simply a mirror image of the median IDA curve that is inferred from the damaged SPO curve shifted to have zero residual roof drift.

Also shown in Figure 10(b) are the median residual/intact capacities versus median residual roof drifts computed via the dynamic approach. Recall that the largest median residual roof drift (and smallest capacity) in each damage state is observed for the bilinear building model. From the dynamic results, it appears that the median residual capacity approaches the median *intact* capacity as the median residual roof drift approaches zero. Although not presented in this paper, this is also observed if the residual roof drift caused by each of the 30 mainshocks considered is plotted against the median residual capacity across the 30 potential aftershocks. Unlike these dynamic results, the static results in Figure 10(b) for DS3 suggest that the median residual capacity is greater than the median intact capacity if the residual roof drift is small. Correcting for this discrepancy is the next step of the calibrated static approach.
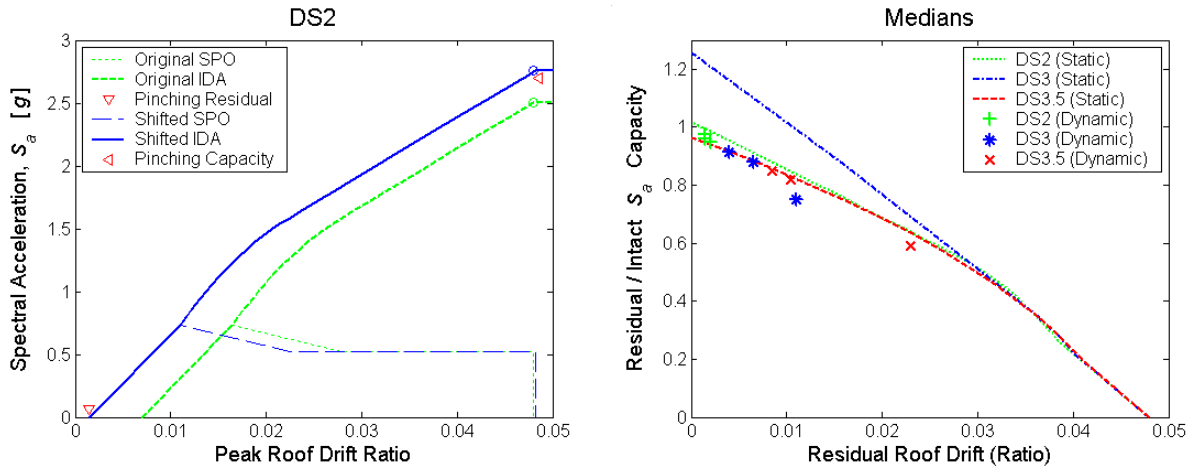

Figure 10. Median residual capacities after Step 2 of the calibrated static approach, i.e., shifting the SPO curve for each post-mainshock damage state to the expected (or measured) residual roof drift. Panel (a) shows an example for the pinching building model in DS2. Panel (b) shows the results for the range of potential residual roof drifts, and compares them with the dynamic results.
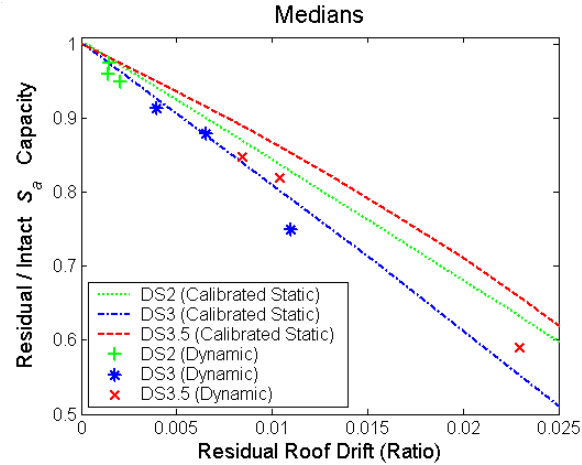
Figure 11. **Median residual (normalized by intact) capacities computed via the calibrated static approach for a given residual roof drift. For DS3.5, the curve matches the results of the dynamic approach more closely if the updated "all periods" version of SPO2IDA [16] is used.**

Step 3: Scale median residual capacity for each post-mainshock damage state

In order to be consistent with the dynamic results when there is no residual roof drift, the median residual/intact capacities computed in Step 2 over the range of potential residual roof drifts [see Figure 10(b)] are divided by their value at zero residual roof drift. A close-up of the resulting median residual/intact capacities plotted against the residual roof drifts is shown in Figure 11. As a result of this scaling, the median residual capacity is equal to the median intact capacity when the residual roof drift is zero, consistent with the trend of the dynamic results also shown in the figure.

The errors in the median residual/intact capacities computed via the calibrated static approach, expressed as percentages of the dynamic results, are enumerated in Table 6. Here the residual roof drifts assumed for the calibrated static approach are the median values computed via NDA of the three building models (see Figure 8 above). Compared to the errors from the "un-calibrated" static approach (see Table 5 above), the errors from the calibrated approach are smaller for all of the building models in DS2 through DS3.5. In fact, the errors are less than about 5%, except for the bilinear building model in DS3.5. For all three of the building models in DS3.5, the errors can be reduced further (to less than 2.3%), without affecting much the errors for DS2 and DS3, if one uses the version of SPO2IDA that covers "all periods" [16] instead of just "moderate periods." The latter is used in this paper merely to be consistent with the case studies presented in the guidelines by Bazzurro *et al.* [6], which are being updated to incorporate the calibrated static approach. Using the updated "all periods" version of SPO2IDA, the median residual capacities computed via the calibrated static approach have been found to be within about 5% of those computed via the dynamic approach for three other SDOF building models and an MDOF model of the case-study building.

Table 6. **Error in the median residual (normalized by intact) capacities computed via the calibrated static approach, expressed as a percentage of the more accurate dynamic results also shown in Figure 11.**

Building Model	Error in Median Residual/Intact Capacity from Calibrated Static Computation				
	DS1 (Intact)	DS2	DS3	DS3.5	DS4 (Collapsed)
Bilinear	0	2.4%	5.6%	11.5%	--
Peak-Oriented	0	2.4%	-0.3%	5.1%	--
Pinching	0	0.7%	1.5%	4.8%	--

Summary of steps for calibrated static computation
Subsequent to obtaining an SPO curve for the building in each post-mainshock damage state (i.e., Step 1 of the "un-calibrated" static approach), the additional steps involved in the "calibrated" static computation of median residual capacity can be summarized as follows:

2a. Shift the SPO curve for each post-mainshock damage state to be consistent with the expected (or measured, as discussed below) residual roof drift, and compute the resulting median residual capacity using SPO2IDA.
2b. Repeat Step 2a supposing no (i.e., zero) residual roof drift.
3. Divide the median residual capacities computed in Step 2a by the corresponding median residual capacities compute in Step 2b, and multiply by the median intact capacity (i.e., the median residual capacity for DS1, which has no residual roof drift). If, in fact, the residual roof drift is zero, the resulting median residual capacity for each damage state will equal the median intact capacity, consistent with the results of dynamic analyses.

Left open is the matter of determining the "expected" residual roof drift used in Step 2a. In the demonstration of the calibrated static approach above, recall that the expected residual roof drifts were set equal to the median residual roof drifts computed via NDA's of the three building models. Needless to say, NDA's are not carried out in the calibrated static approach, but expected residual roof drifts can be estimated from generic NDA results. For example, results like those in Figure 8 above, or from other researchers, e.g. [15,17], can be used to estimate the expected residual roof drift as a fraction of the peak roof drift associated with each damage state. Alternatively, but also based on NDA results, the expected residual roof drift could be estimated as a fraction of the residual roof drift implied by the SPO curve for each damage state (before shifting). As mentioned in Step 2a, even the residual roof drift measured in the field could be used. In this case, the median residual capacity for each post-mainshock damage state should be computed prior to the mainshock for a range of potential residual roof drifts, like in Figure 11 above.

CONCLUSIONS

Based on the results of back-to-back mainshock-aftershock nonlinear dynamic analyses (NDA's) of case-study building models, a "calibrated" static approach is developed for computing the median residual capacity of a mainshock-damaged building in terms of the aftershock ground motion it can withstand without collapsing. As originally proposed by Bazzurro *et. al.* [6], the static computation involves static pushover (SPO) analysis and use of the SPO2IDA spreadsheet tool [7,8] to infer the corresponding dynamic capacity. The "calibrated" computation takes into account the residual roof drift of the mainshock-damaged building, as either (i) measured in the field or (ii) expected for the observed state of damage based on, for example, generic research results of NDA's of buildings. The calibration also reflects the observation from the mainshock-aftershock dynamic computations that, as the residual roof drift approaches zero, the median residual capacity approaches the median capacity of the building in its undamaged state. Without the calibration, the static computation of median residual capacity is observed to underestimate the more accurate results of the dynamic computation. In fact, the median residual capacities computed via the dynamic approach in this paper (for the case-study building models over a range of potential post-mainshock damage states) may seem to some to be surprisingly small considering the degradation in strength and stiffness. This resilience of mainshock-damaged buildings has also been observed by other researchers, e.g., [3,4], and is somewhat corroborated by the historical rarity of aftershock-induced collapses. Given the economic and other costs associated with restricted or denied occupancy (i.e., yellow or red tags), it is important that the residual capacities of mainshock-damaged buildings be computed accurately. To this end, both the calibrated static and dynamic approaches to computing residual capacities should be investigated further.

REFERENCES

1. Yeo GL, Cornell CA. "Building tagging criteria based on aftershock PSHA." Proceeding of the 13WCEE, Vancouver, Canada. Paper No. 3283. August, 2004.
2. SAC Joint Venture. "FEMA 352: Recommended post-earthquake evaluation and repair criteria for welded steel moment-frame buildings." Sacramento, California. 2000.
3. Lee K, Foutch DA. "Performance evaluation of damaged steel frame buildings subjected to seismic loads." ASCE Journal of Structural Engineering 2004; 130(4): 588-599.
4. Amadio C, Fragiacomo M, Rajgelj S. "The effects of repeated earthquake ground motions on the non-linear response of SDOF systems." Earthquake Engineering and Structural Dynamics 2003; 32: 291-308.
5. Luco N, Cornell CA, Yeo GL. "Annual limit-state frequencies for partially-inspected earthquake-damaged buildings." Structural Safety 2002; 24: 281-296.
6. Bazzurro P, Cornell CA, Menun C, Motahari M. "Advanced seismic assessment guidelines." PEER Report Draft. February, 2003.
7. Vamvatsikos D, Cornell CA. "Practical estimation of the seismic demand and capacity of oscillators with multi-linear static pushovers through incremental dynamic analysis." Proceeding of the 7th U.S. National Conference on Earthquake Engineering, Boston, MA. July, 2002.
8. Vamvatsikos D, Cornell CA. "Direct estimation of the seismic demand and capacity of MDOF systems through Incremental Dynamic Analysis of an SDOF approximation." ASCE Journal of Structural Engineering (to be published).
9. Bazzurro P, Cornell CA, Menun C, Motahari M. "Guidelines for seismic assessment of damaged buildings." Proceeding of the 13WCEE, Vancouver, Canada. Paper No. 1708. August, 2004.
10. RAM International. "RAM Perform 2D Software, V1.04." Carlsbad, CA. October, 2000.
11. Clough RW. "Effect of stiffness degradation of earthquake ductility requirements." Report No. 66-16, Department of Civil Engineering, University of California, Berkeley. 1996.
12. Krawinkler H, Rahnama M, Gupta A, Miranda M, Ayoub A, Ibarra L. "SNAP: SDOF nonlinear analysis program." Stanford University, Stanford, CA. October, 2002.
13. Mahin SA, Bertero VV. "An evaluation of inelastic seismic design spectra." ASCE Journal of Structural Engineering 1981; 107(ST9): 1777-1795.
14. Christopoulos C, Pampanin S, Priestley MJN. "Performance-based seismic response of frame structures including residual deformations. Part I: Single-degree of freedom systems." Journal of Earthquake Engineering 2003; 7(1): 97-118.
15. Ruiz-Garcia J (under the direction of Miranda E). "Performance-based evaluation of existing structures accounting for residual displacements" (Personal communication). PhD dissertation, Department of Civil and Environmental Engineering, Stanford University, Stanford, CA. Expected date of completion: December, 2004.
16. Vamvatsikos D. "SPO2IDA: All periods" (Excel spreadsheet). Available from http://tremble.stanford.edu/nausika/software/spo2ida-allt.xls as of March, 2004.
17. Pampanin S, Christopoulos C, Priestley MJN. "Performance-based seismic response of frame structures including residual deformations. Part II: Multi-degree of freedom systems." Journal of Earthquake Engineering 2003; 7(1):119-147.